Journal of Solid State Chemistry **142,** 266–272 (1999)
Article ID jssc.1998.7979, available online at http://www.idealibrary.com on IDEAL®

The Praseodymium Zinc Arsenide $Pr_3Zn_2As_6$: Crystallizing with a Vacancy Variant of the $HfCuSi_2$ Type Structure

André T. Nientiedt and Wolfgang Jeitschko

Anorganisch-Chemisches Institut, Universität Münster, Wilhelm-Klemm-Str. 8, D-48149 Münster, Germany

Received March 9, 1998; in revised form July 27, 1998; accepted August 3, 1998

The new compound $Pr_3Zn_2As_6$ has been prepared by reaction of the elemental components in a NaCl–KCl flux. It crystallizes with a very pronounced subcell of the $HfCuSi_2$ type structure with two formula units $PrZn_{2/3}As_2$ in the tetragonal subcell with $a = 400.6(1)$ pm and $c = 1019.7(4)$ pm. The ordered distribution of occupied and unoccüpied zinc positions leads to a three times larger cell. This structure was determined from four-circle X-ray diffractometer data of a twinned crystal: *Pmmn*, $a = 399.89(9)$ pm, $b = 1204.2(3)$ pm, $c = 1019.7(4)$ pm, $Z = 2$, $R = 0.039$ for 2663 structure factors and 39 variable parameters. Chemical bonding in this compound is briefly discussed.

INTRODUCTION

A large number of ternary compounds with the tetragonal $HfCuSi_2$ type structure (1), a ternary variant of the ZrCuSiAs type structure (2), are known. Pearson's Handbook (3) lists more than a dozen such compounds, e.g., $ZrCuSi_2$, $HfCuGe_2$, $UCuAs_2$, $LaTSb_2$ (T = Mn, Co, Cu, Zn), and $CaMnBi_2$. In addition, some rare earth (*Ln*) series with this structure have been reported recently: $LnCuAs_2$ (4), $LnMnSb_2$ (5, 6), $LnFeSb_2$ (7), $LnCoSb_2$ (6, 7), $LnNiSb_2$ (8, 9), $LnPdSb_2$ (8), $LnCuSb_2$ (8), $LnAgSb_2$ (4, 10), $LnAuSb_2$ (6, 8), $LnZnSb_2$ (5, 6), and $LnCdSb_2$ (5, 6). Single-crystal structure determinations of the antimonides $CeAgSb_2$ (4, 10) and $LaAuSb_2$ (6) showed that all atomic positions are fully occupied. In contrast, the structure refinements of three different crystals of the compound $LaMn_{1-x}Sb_2$ showed considerable defects for the manganese position: $LaMn_{0.65}Sb_2$ (11), $LaMn_{0.71(1)}Sb_2$ (6), and $LaMn_{0.76}Sb_2$ (11). Similar defects were found during the structure refinements of $LaCo_{0.68}Sb_2$ (11), $LaCu_{0.82}Sb_2$ (11), $LaCu_{0.87}Sb_2$ (11), $LaZn_{0.52}Sb_2$ (11), and $LaCd_{0.700(5)}Sb_2$ (6). The presently reported structure determination of $Pr_3Zn_2As_6$ is the first one where the defects at the transition metal site were found to be ordered.

SAMPLE PREPARATION AND LATTICE CONSTANTS

The samples of $Pr_3Zn_2As_6$ were obtained by reaction of the elemental components in a NaCl–KCl flux. Filings of praseodymium (nominal purity 99.9%) were prepared under dry (Na) paraffin oil, which subsequently was washed out with dry hexane. The filings were stored under vacuum and were only briefly exposed to air prior to the reactions. Zinc (Merck, 99.9%) was purchased as a powder. The arsenic (coarse grains, 99%) was purified by fractional sublimation under reduced argon pressure. First the trioxide As_2O_3 was sublimed with the hot end of the sealed silica tube at 300°C and the other end at room temperature. After separation of this cold end, containing the trioxide, the tube was sealed again, and the arsenic was sublimed with the hot end of the tube at 600°C.

The elements had the atomic ratio Pr:Zn:As = 1:1:2 and 500 mg of this mixture was sealed in an evacuated silica tube together with 2 g of the NaCl–KCl (1:1) flux. The annealing was for 1 day at 500°C and 5 days at 800°C, followed by quenching in air. The salt matrix was dissolved with water, which does not attack the shiny black crystals of $Pr_3Zn_2As_6$. The powdered product is black and stable in air for a long time. Small amounts of a second phase were observed in the Guinier powder diagrams, which were not identified. The crystals of $Pr_3Zn_2As_6$ were investigated in a scanning electron microscope. An energy-dispersive X-ray fluorescence analysis did not reveal any impurity elements heavier than sodium.

A Guinier powder diagram of the product was recorded using $CuK\alpha_1$ radiation with α-quartz ($a = 491.30$ pm, $c = 540.46$ pm) as an internal standard. The pattern was recognized to be similar to those of $LaMn_{0.71}Sb_2$ and $LaCd_{0.70}Sb_2$ (6) with tetragonal $HfCuSi_2$ type structure. A least-squares fit of these powder data resulted in the tetragonal lattice constants $a = 400.6(1)$ pm and $c = 1019.7(4)$ pm. After the correct superstructure had been obtained from the single-crystal investigation, a careful inspection of the powder diagram revealed the splitting of

0022-4596/99 $30.00

several diffraction lines. These were assigned the proper indices by comparing the observed pattern with the calculated one (12), using the positional parameters of the refined structure. The following orthorhombic lattice constants were obtained: $a = 399.89$ (9) pm, $b = 1204.2(3)$ pm, $c = 1019.7(4)$ pm. These compare well with the ones measured on the single-crystal diffractometer using only well-resolved superstructure reflections: $a = 399.33(3)$ pm, $b = 1202.7(2)$ pm, $c = 1018.2(1)$ pm. However, since the single-crystal data are affected by systematic errors due to absorption, we consider those from the Guinier powder data to be more accurate.

STRUCTURE DETERMINATION

X-ray intensity data for the structure determination were collected on an Enraf-Nonius CAD4 single-crystal diffractometer with graphite-monochromated Mo$K\alpha$ radiation and a scintillation counter with pulse-height discrimination. The background was determined at both ends of each θ–2θ scan and an absorption correction was applied using ψ-scan data. Further details are summarized in Table 1.

The intensity data were collected from a twinned crystal with pseudotetragonal symmetry and the lattice constants $a = 1200(1)$ pm and $c = 1017(2)$ pm. The reciprocal lattice of this crystal showed a very pronounced subcell of tetragonal symmetry, which corresponds to the $HfCuSi_2$ type structure (1). This subcell was refined first with a full-matrix least-squares program as provided by the SHELXL-93 package (13), using atomic scattering factors as provided by the program. The weighting scheme accounted for the counting statistics, and a parameter correcting for isotropic secondary extinction was optimized as a least-squares variable. The zinc position was found to have very large thermal parameters. A refinement of the occupancy parameter for this position together with anisotropic thermal parameters resulted in an occupancy of only two-thirds.

The determination of the superstructure was not straightforward, since the correct orthorhombic cell was not immediately recognized. The reciprocal lattice of the large pseudotetragonal cell described above showed systematic non-space group extinctions, which eventually could be rationalized by the superposition of two twin domains of an orthorhombic lattice as shown in Fig. 1. This orthorhombic cell has a three times larger volume than the tetragonal subcell. A proposal for the superstructure was worked out for the nonisomorphic subgroup *Pmmn*, assuming that occupied and unoccupied zinc positions are responsible for the superstructure. The space group relationships and the proper cell transformation from the tetragonal subcell to the orthorhombic superstructure are shown in Fig. 2. This structure proposal was readily refined by the full-matrix least-squares program as described above. In a separate series of least-squares cycles, the occupancy factors were refined together with the thermal parameters. All occupancy values were within 2% of the ideal composition (Table 2). The only exception was the occupied zinc position, which showed an occupancy of 95.8% with a standard deviation of

TABLE 1
Crystallographic Data for the Subcell ($PrZn_{2/3}As_2$) and the Superstructure of $Pr_3Zn_2As_6$

	Subcell	Superstructure
Structure type	$HfCuSi_2$	$Pr_3Zn_2As_6$
Space group	*P4/nmm* (No. 129)	*Pmmn* (No. 59)
Cell constants (pm)	$a = 400.6(1)$	$a = 399.89(9)$
		$b = 1204.2(3)$
	$c = 1019.7(4)$	$c = 1019.7(4)$
Cell volume (nm^3)	0.16364	0.4910
Formula units per cell	$Z = 2$	$Z = 2$
Formula mass	334.34	1003.01
Calculated density (g/cm^3)	$\rho_{calc} = 6.78$	$\rho_{calc} = 6.78$
Crystal size (μm^3)	$50 \times 50 \times 25$	$50 \times 50 \times 25$
Scan range	$4^\circ < 2\theta < 80^\circ$	$4^\circ < 2\theta < 80^\circ$
Range in *h*, *k*, *l*	± 7, 0–7, ± 18	± 7, 0–21, ± 18
Highest/lowest transmission	2.47	2.47
Total number of reflections	6253	8166
Inner residual (on F^2 values)	$R_i = 0.051$	
Unique reflections with $I > 2\sigma(I)$	309	2663
Number of variables	16	39
Conventional residual with $F > 2\sigma(F)$	$R = 0.018$	$R = 0.039$
Twin ratio		0.580(5)/0.420(5)
Highest residual density ($e/Å^3$)	2.46	3.34

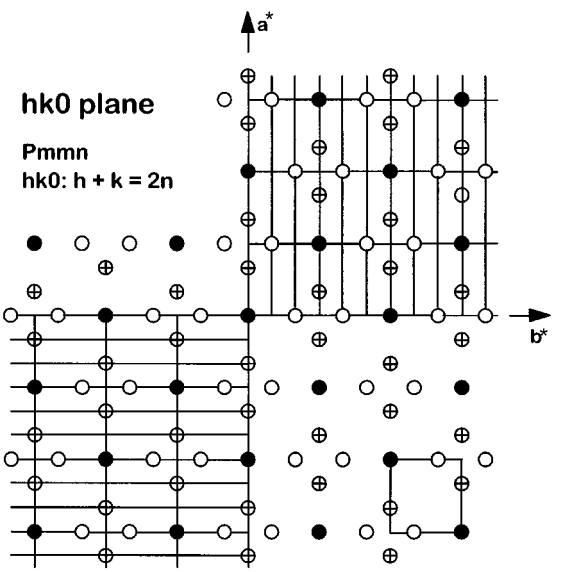

FIG. 1. Reciprocal lattice plane *hk*0 of a twin of $Pr_3Zn_2As_6$. Black dots represent strong reflections corresponding to the tetragonal $HfCuSi_2$ type *P4/nmm* subcell, which is outlined in the lower right-hand part of the figure. Open circles and crossed circles represent the superstructure reflections of the two twin domains.

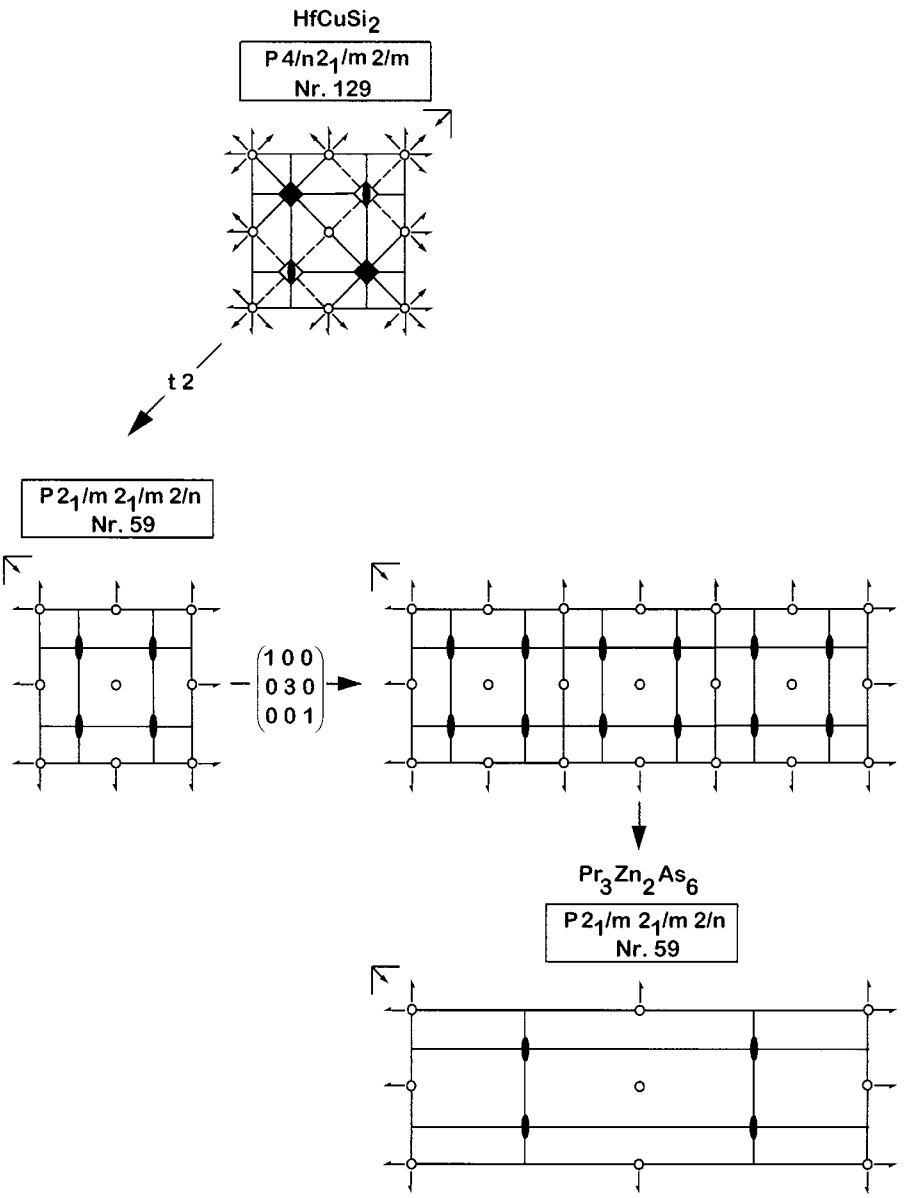

FIG. 2. Group–subgroup relationships of the tetragonal $HfCuSi_2$ type subcell and the orthorhombic superstructure of $Pr_3Zn_2As_6$.

0.6%. It seems possible that even this occupied zinc site has some defects. However, since these defects amount to only 7 standard deviations, we preferred the full occupancy of this site in the final refinement cycles.

The results are summarized in Tables 1–3 together with the results obtained for the refinement of the tetragonal subcell. The structure factor tables are available from the authors (15). Figure 3 shows the structure of the subcell and the superstructure. The subcell was also refined with split zinc positions and isotropic thermal parameters. These split positions are indicated for one zinc site in the upper right-hand part of Fig. 3.

DISCUSSION

The present structure determination for the new arsenide $Pr_3Zn_2As_6$ is the first for a compound with an $HfCuSi_2$ type subcell. Other superstructures can be expected for $HfCuSi_2$ type compounds whenever the late transition metal (Cu) site is found with deviations from the full occupancy. However, superstructure reflections can only be expected if occupied and nonoccupied transition metal sites have long-range order. In $Pr_3Zn_2As_6$, annealing for 1 week at 800°C was enough to establish this order.

TABLE 2
Atomic Parameters of $Pr_3Zn_2As_6$[a]

Atom	Position	Occupancy	x	y	z	U_{11}	U_{22}	U_{33}	$U_{12}=U_{13}$	U_{23}	U_{eq}
					$HfCuSi_2$ type subcell for $PrZn_{2/3}As_2$ (space group $P4/nmm$)						
Pr	2*c*	0.998(4)	1/4	1/4	0.27012(3)	75(1)	U_{11}	80(1)	0	0	77(1)
Zn	2*a*	0.661(5)	3/4	1/4	0	260(4)	U_{11}	60(4)	0	0	193(3)
As1	2*b*	1.001(5)	3/4	1/4	1/2	149(2)	U_{11}	62(4)	0	0	120(1)
As2	2*c*	1.006(5)	1/4	1/4	0.84470(7)	74(2)	U_{11}	117(3)	0	0	88(1)
					Superstructure of $Pr_3Zn_2As_6$ (space group $Pmmn$)						
Pr1	4*e*	1.001(4)	1/4	0.58723(4)	0.72821 (4)	48(2)	84(3)	76(2)	0	1(2)	69(1)
Pr2	2*a*	1.005(5)	1/4	1/4	0.73311(8)	51(4)	82(3)	71(3)	0	0	68(1)
Zn	4*e*	0.958(6)	1/4	0.0968(1)	0.0038(2)	104(4)	138(5)	50(4)	0	36(5)	97(2)
□	2*b*		1/4	3/4	0						
As1	4*e*	1.007(6)	1/4	0.08319(8)	0.5024(2)	133(6)	157(6)	56(3)	0	5(5)	115(2)
As2	4*e*	1.011(6)	1/4	0.58207(8)	0.15176(9)	40(5)	95(5)	84(3)	0	13(3)	73(1)
As3	2*b*	1.000(8)	1/4	3/4	0.4958(3)	139(7)	150(7)	38(5)	0	0	109(2)
As4	2*a*	1.014(8)	1/4	1/4	0.1629(2)	56(7)	86(6)	94(6)	0	0	79(2)

[a] Standard deviations in the positions of the least significant digits are given in parentheses throughout the paper. The positional parameters of the superstructure were standardized using the program STRUCTURE TIDY (14). The occupancy parameters were varied in separate least-squares cycles along with the thermal parameters. In the final cycles the ideal occupancies were assumed (for the zinc position of the subcell this is 2/3). The thermal paramters are in units of pm^2. They are of the form $U_{ij} = \exp[-2\pi^2\{h^2a^{*2}U_{11} + \cdots + 2klb^*c^*U_{23}\}]$. The vacant zinc site of the superstructure is indicated by the symbol □.

TABLE 3
Interatomic Distances in $Pr_3Zn_2As_6$[a]

Subcell ($PrZn_{2/3}As_2$)			Superstructure ($Pr_3Zn_2As_6$)					
Pr:	4As2	306.6	Pr1:	2As4	301.2	Pr2:	2As3	307.3
	4As1	308.4		1As3	307.6		4As2	307.7
	4(2/3)Zn	340.6		1As1	308.5		2As1	309.4
				2As1	308.7		2Zn	332.0
				2As2	310.7		2□	337.7
				2Zn	338.8			
				1□	339.4			
				1Zn	357.9			
Zn:	4As2	255.4	Zn:	1As4	245.7	□:	2As2	254.6
	4(2/3)Zn	283.3		2As2	255.8		2As4	259.9
	4Pr	340.6		1As2	262.9		4Zn	272.1
				2□	272.1		2Pr2	337.7
				2Zn	307.1		2Pr1	339.4
				1Pr2	332.0			
				2Pr1	338.8			
				1Pr1	357.8			
As1:	4As1	283.3	As1:	2As1	283.1	As3:	4As1	283.4
	4Pr	308.4		2As3	283.4		2Pr2	307.3
				1Pr1	308.5		2Pr1	307.6
				2Pr1	308.7			
				1Pr2	309.4			
As2:	4(2/3)Zn	255.4	As2:	1□	254.6	As4:	2Zn	245.7
	4Pr	306.6		2Zn	255.8		2□	259.9
				1Zn	262.9		4Pr1	301.2
				2Pr2	307.7			
				2Pr1	310.7			

[a] The unoccupied zinc position of the superstructure is indicated by the symbol □. All distances shorter than 390 pm (Pr–Pr, Pr–Zn, Pr–As) or 360 pm (Zn–Zn, Zn–As, As–As), respectively, are listed. Standard deviations are all 0.2 pm or less.

The tetragonal $HfCuSi_2$ type subcell of $Pr_3Zn_2As_6$ (upper part of Fig. 3) may be considered to consist of two kinds of atomic layers extending perpedicular to the tetragonal c axis. One layer has the As1 atoms at $z = 1/2$ at its center. They form a square grid with praseodymium atoms above and below the arsenic squares alternating in the manner of a checkerboard. This layer with the composition PrAs has some ionic character. The other layer consists of the zinc positions, with an occupancy of two-thirds, and the As2 atoms. This layer has a more covalent character with the composition $Zn_{2/3}As$. In this layer the zinc atoms are in the center with arsenic atoms above and below, again alternating in a checkerboard-like manner.

The three times larger superstructure (lower part of Fig. 3) arises through the ordered arrangement of voids and zinc atoms within the $Zn_{2/3}As$ layers. The PrAs layers are only marginally affected by this order.

The coordination polyhedra of the subcell and the superstructure are compared in Fig. 4. In the subcell praseodymium atoms are located in a square antiprism of arsenic atoms, which is capped by four zinc positions with an occupancy of two-thirds, i.e., by an average of 2.67 zinc atoms. Accordingly, in the superstructure the corresponding coordination polyhedra of the Pr1 and Pr2 atoms contain three or two zinc atoms, respectively.

The partially occupied zinc position of the subcell is coordinated by four arsenic atoms forming a slightly stretched tetrahedron [As–Zn–As angles: $4 \times 112.60(2)^\circ$ and $2 \times 103.39(5)^\circ$]. The Zn–As distance of 255.4 pm in the subcell and the average Zn–As distance of 255.1 pm in the superstructure have practically the same lengths as the

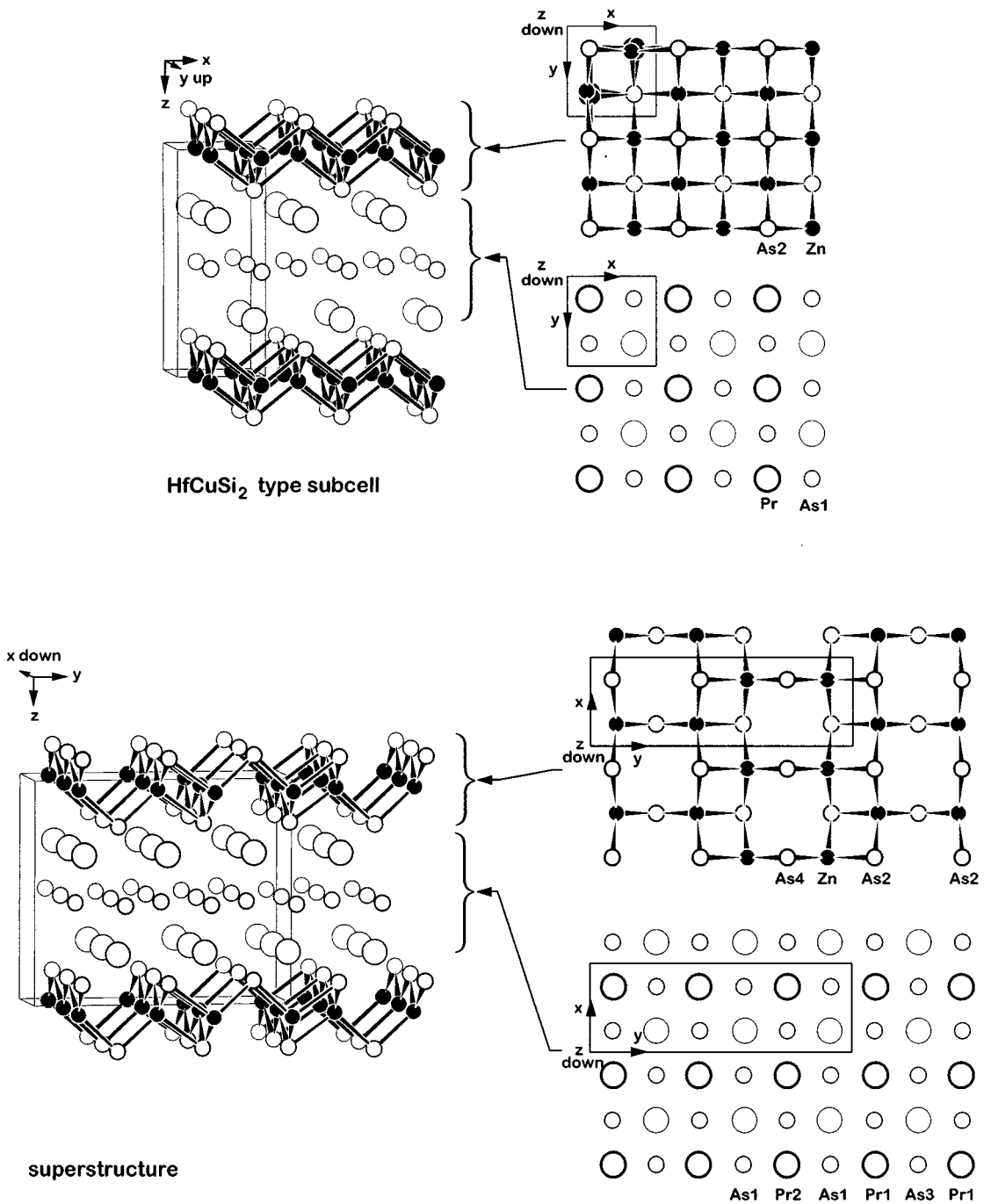

FIG. 3. Structure of $Pr_3Zn_2As_6$. In the upper part of the figure the tetragonal $HfCuSi_2$ type subcell is shown. The zinc positions have an occupancy of 2/3. In the three times larger orthorhombic superstructure voids and occupied zinc positions are ordered. The PrAs and ZnAs layers are indicated; in the right-hand parts of the figure they are projected along directions perpendicular to the layers.

average Zn–As distance of 256.1 pm in Zn_3As_2 (16). In the superstructure the unoccupied zinc site has the same coordination as the zinc position of the subcell, whereas the occupied zinc site has two unoccupied zinc positions in its coordination. The Zn–Zn distances of 307.1 pm between the occupied zinc positions must be considered as essentially nonbonding distances in view of the fact that the zinc atoms have their valence electrons involved in Zn–As bonding and the Zn–Zn distances in elemental zinc (6×264.4 pm and 6×291.2 pm) are considerably smaller (17). In contrast, the

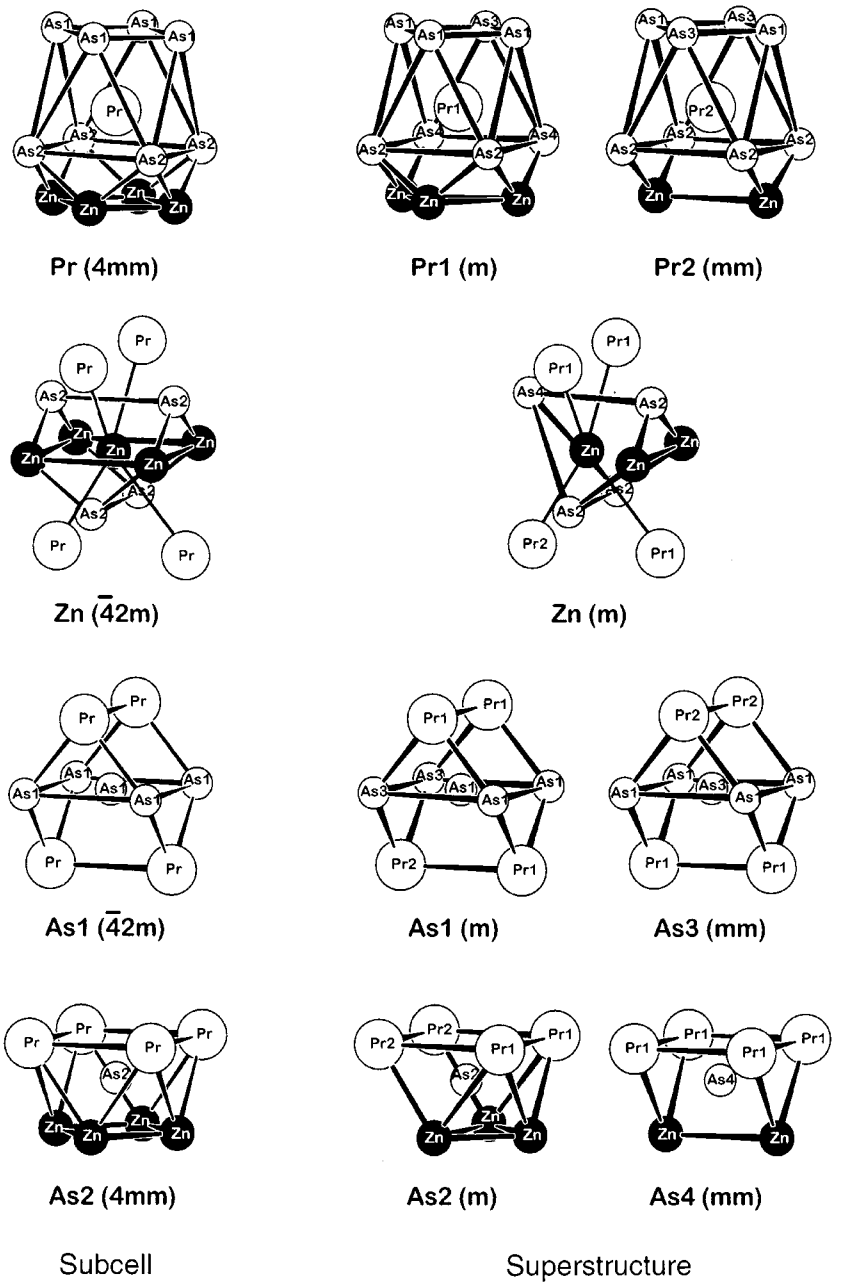

FIG. 4. Coordination polyhedra of $Pr_3Zn_2As_6$ in the subcell (left-hand side) and in the superstructure. The site symmetries are indicated in parentheses.

unoccupied zinc site has four zinc neighbors at the relatively short distance of 272.1 pm. Apparently, one reason for these sites to remain unoccupied seems to be the fact that these interactions would be antibonding.

The As1 atoms of the subcell correspond to the As1 and As3 atoms of the superstructure, and they all have the same coordination. They are situated in the center of a square of arsenic atoms with As–As distances of 283.3 pm in the subcell, which are practically unchanged in the superstructure. These distances are considerably greater than the two-electron bond distance of 251.7 pm in the α-modification of elemental arsenic (17); nevertheless, these As–As interactions must be considered as weakly bonding as will be discussed below. The As2 position of the subcell is coordinated by a square of partially occupied zinc positions and a square of praseodymium atoms. Together these two squares form an antiprism. In the superstructure the corresponding As2 and As4 atoms have only three and two zinc

neighbors, respectively, with (average) As–Zn distances of 258.2 and 245.7 pm, thus reflecting the lower coordination number of the As4 atoms.

To rationalize chemical bonding, we may start from simple concepts. The praseodymium atoms have three valenced electrons. Since there are no short Pr–Pr distances and since the praseodymium atoms are the most electropositive components of the compound, these electrons will be involved in bonding toward the arsenic atoms and consequently the praseodymium atoms obtain the oxidation number $+3$. Similarly the zinc atoms have two valence electrons, and since we assumed the Zn–Zn distances of 307.1 pm to be nonbonding, the zinc atoms obtain the oxidation number $+2$. The arsenic atoms are the most electronegative components of the compound, and we can therefore assume that they use their 4*s* and 4*p* orbitals completely for bonding or nonbonding interactions (octet rule). The As2 and As4 atoms do not form any As–As bonds. Therefore they obtain the oxidation number -3. On the other hand, the As1 and As3 atoms are close enough to each other to form bonding As–As interactions. These therefore have to balance the oxidation numbers and we arrive at the formula $(Pr^{3+})_3(Zn^{2+})_2(As1^{1.33-})_2(As2^{3-})_2As3^{1.33-}$ $As4^{3-}$, which also takes care of the fact that the As1 and As3 atoms have practically the same atomic environments. Simple arithmetic shows (in agreement with the octet rule, the arsenic atoms in elemental arsenic $As^{0\pm}$ form three two-electron As–As bonds, As^{1-} has four electrons involved in As–As bonding, As^{2-} has two electrons forming As–As bonds, and As^{3-} has none) that each of the As1 and As3 atoms with the oxidation number -1.33 has $3\frac{1}{3}$ (shared) electrons available for As–As bonding. Since each of these arsenic atoms has four arsenic neighbors (with As1–As1 and As1–As3 distances of 283.1 and 283.4 pm, respectively), each of these As–As interactions obtains a bond order of $3.33/8 = 0.416$. In other words, it follows from this simple bonding model, that each of the As1 and As3 atoms has $3\frac{1}{3}$ electrons involved in As–As bonding and $4\frac{2}{3}$ electrons involved in bonding toward the metal atoms.

Summing up, we believe that the vacancies at the zinc sites of the $HfCuSi_2$ type subcell of $Pr_3Zn_2As_6$ are formed to avoid antibonding Zn–Zn interactions. The number of these vacancies has to reflect the requirements of the As–As bonding interactions.

ACKNOWLEDGMENTS

We thank Dipl.-Ing. U. Ch. Rodewald for the very competent data collection and the determination of the lattice constants on the four-circle diffractometer. We also acknowledge Dr. R.-D. Hoffmann for helpful discussion concerning the twinning and K. Wagner for the work with the scanning electron microscope. We are also grateful for a generous gift of silica tubes (Dr. G. Höfer, Heraeus Quarzschmelze Hanau). This work was supported by the Deutsche Forschungsgemeinschaft and the Fonds der Chemischen Industrie.

REFERENCES

1. L. S. Andrukhiv, L. A. Lysenko, Ya. P. Yarmolyuk, and E. I. Gladyshevskii, *Dopov. Akad. Nauk Ukr. RSR, Ser. A* 645 (1975).
2. V. Johnson and W. Jeitschko, *J. Solid State Chem.* **11,** 161 (1974).
3. P. Villars and L. D. Calvert, "Pearson's Handbook of Crystallographic Data for Intermetallic Phases." ASM International, Materials Park, OH, 1991.
4. M. Brylak, M. H. Möller, and W. Jeitschko, *J. Solid State Chem.* **115,** 305 (1995).
5. O. Sologub, K. Hiebl, P. Rogl, and O. Bodak, *J. Alloys Compd.* **227,** 40 (1995).
6. P. Wollesen, W. Jeitschko, M. Brylak, and L. Dietrich, *J. Alloys Compd.* **245,** L5 (1996).
7. A. Leithe-Jasper and P. Rogl, *J. Alloys Compd.* **203,** 133 (1994).
8. O. Sologub, K. Hiebl, P. Rogl, H. Noël, and O. Bodak, *J. Alloys Compd.* **210,** 153 (1994).
9. G. André, F. Bourée, A. Oleś, B. Penc, W. Sikora, A. Szytuła, and A. Zygmunt, *J. Alloys Compd.* **255,** 31 (1997).
10. O. Sologub, H. Noël, A. Leithe-Jasper, P. Rogl, and O. I. Bodak, *J. Solid State Chem.* **115,** 441 (1995).
11. G. Cordier, H. Schäfer, and P. Woll, *Z. Naturforsch., B* **40,** 1097 (1985).
12. K. Yvon, W. Jeitschko, and E. Parthé, *J. Appl. Crystallogr.* **10,** 73 (1977).
13. G. M. Sheldrick, SHELX-93, Program for Crystal Structure Refinement, University of Göttingen, Germany, 1993.
14. L. M. Gelato and E. Parthé, *J. Appl. Crystallogr.* **20,** 139 (1987).
15. A. T. Nientiedt, Doctoral Thesis, Universität Münster, Germany, 1997.
16. A. Pietraszko and K. Lukaszewicz, *Bull. Acad. Pol. Sci., Ser. Sci. Chim.* **24,** 459 (1976).
17. J. Donohue, "The Structures of the Elements." Wiley, New York, 1974.